JOURNAL OF APPLIED PHYSICS **116**, 184507 (2014)

Gate-control efficiency and interface state density evaluated from capacitance-frequency-temperature mapping for GaN-based metal-insulator-semiconductor devices

Hong-An Shih, Masahiro Kudo, and Toshi-kazu Suzuki[a)]
Center for Nano Materials and Technology, Japan Advanced Institute of Science and Technology (JAIST), 1-1 Asahidai, Nomi, Ishikawa 923-1292, Japan

(Received 29 September 2014; accepted 28 October 2014; published online 14 November 2014)

We present an analysis method for GaN-based metal-insulator-semiconductor (MIS) devices by using capacitance-frequency-temperature (*C-f-T*) mapping to evaluate the gate-control efficiency and the interface state density, both exhibiting correlations with the linear-region intrinsic transconductance. The effectiveness of the method was exemplified by application to AlN/AlGaN/GaN MIS devices to elucidate the properties of AlN-AlGaN interfaces depending on their formation processes. Using the *C-f-T* mapping, we extract the gate-bias-dependent activation energy with its derivative giving the gate-control efficiency, from which we evaluate the AlN-AlGaN interface state density through the Lehovec equivalent circuit in the DC limit. It is shown that the gate-control efficiency and the interface state density have correlations with the linear-region intrinsic transconductance, all depending on the interface formation processes. In addition, we give characterization of the AlN-AlGaN interfaces by using X-ray photoelectron spectroscopy, in relation with the results of the analysis. © *2014 AIP Publishing LLC*. [http://dx.doi.org/10.1063/1.4901290]

I. INTRODUCTION

GaN-based metal-insulator-semiconductor (MIS) devices, represented by AlGaN/GaN MIS heterojunction field-effect transistors, have attracted much attention for their potential uses in high-frequency and high-power applications. As a gate-insulator of the MIS devices, high-dielectric-constant (high-*k*) oxide materials, such as Al_2O_3,[1] HfO_2,[2,3] and also high-*k* nitride materials, such as AlN,[4–8] BN,[9,10] have been investigated. Owing to their high thermal conductivities, the nitride materials are favorable also for passivation of GaN-based devices, exhibiting good heat release properties.[4,11–15] Since controlling insulator-semiconductor interfaces is critical for both gate-insulator or passivation applications, it is important to characterize and analyze the interface states. In fact, we observe frequency dispersion in *C-V* characteristics of MIS devices, attributed to electron trapping/detrapping at interface mid-gap states leading to gate-control impediment. Such mid-gap states in GaN-based devices have been characterized and analyzed by conductance method,[5,6,16–21] Terman method,[22,23] photo-assisted *C-V* method,[24,25] and deep level transient spectroscopy.[26–29] Although the conductance method is widely used, there are difficulties in the analysis of deep interface states with long trapping time constants[30] in MIS devices based on wide-bandgap materials like GaN.[6,7,31] Also, the analysis results obtained from the conductance method is affected by the assumed value of the insulator capacitance. Previously, as an extension of the conductance method, we proposed a method using capacitance-frequency-temperature (*C-f-T*) mapping[7] obtained from the temperature-dependent *C-V-f* characteristics for GaN-based MIS devices, based on the Lehovec equivalent circuit.[32] From constant-capacitance contours, exhibiting a straight line behavior in the mapping, an activation energy E_a corresponding to an interface state energy level can be extracted for a wide range of gate biases without assuming any parameter. The *C-f-T* mapping helps us to understand deep interface states in wide-bandgap MIS devices, serving as an auxiliary tool to the conventional conductance method.

In this article, by using *C-f-T* mapping, we present an analysis method for GaN-based MIS devices to evaluate the gate-control efficiency and the interface state density, both exhibiting correlations with the linear-region intrinsic transconductance. Employing AlN/AlGaN/GaN MIS devices, where the AlN gate insulator is sputtering-deposited, we elucidate the properties of the AlN-AlGaN interfaces depending on their formation processes to exemplify the effectiveness of the method. Through characterizing the activation energies modulated by the gate biases, we obtain the gate-control efficiency of the MIS devices, i.e., the ratio of the bandbending change in the semiconductor to the total gate voltage change. Even though the Lehovec equivalent circuit is based on an AC small-signal model, we find that its DC limit, described by the insulator capacitance, the semiconductor capacitance, and the interface state density, gives the gate-control efficiency. Therefore, we can evaluate the interface state density from the experimentally obtained gate-control efficiency, using the values of insulator and semiconductor capacitances. From the activation energies corresponding to a wide range of gate biases, we can obtain the gate-control efficiency and the interface state density corresponding to deep interface states in comparison with the conductance method. Moreover, it is shown that the gate-control efficiency and the interface state density have correlations with the linear-region intrinsic transconductance, all depending

[a)]Author to whom correspondence should be addressed. Electronic mail: tosikazu@jaist.ac.jp

on the interface formation processes. In addition, we give characterization of the AlN-AlGaN interfaces by using X-ray photoelectron spectroscopy (XPS), in relation with the results of the analysis.

II. DEVICE FABRICATION

We fabricated AlN/AlGaN/GaN MIS transistors and MIS capacitors simultaneously using an $Al_{0.29}Ga_{0.71}N$ (25 nm)/GaN (3000 nm) heterostructure obtained by metal-organic vapor phase epitaxy on sapphire(0001). Hall-effect measurements of the heterostructure show an as-grown electron mobility $\mu \simeq 1400\,cm^2/V\text{-}s$ and a sheet electron concentration $n_s \simeq 1.0 \times 10^{13}\,cm^{-2}$. On the heterostructure, Ti/Al/Ti/Au Ohmic electrodes were formed and device isolation was achieved by B^+ implantation. To exemplify the effectiveness of the analysis method, we employed AlN/AlGaN/GaN MIS devices with two types of the AlN-AlGaN interface formation processes, by using two types of surface treatments of the AlGaN before the AlN gate insulator deposition. The first type surface treatment includes an organic cleaning by organic solvents and oxygen plasma ashing, and an additional cleaning by an ammonium-based solution, ABS (with cleaning by ABS). The second one includes only the organic cleaning, without the additional cleaning (without cleaning by ABS). The organic solvents and the oxygen plasma ashing were used for removing organic contaminants, whereas the ABS was used with the intention of oxide removal. While the devices without cleaning by ABS were transferred to the sputtering chamber within 15 min after the treatment, the ones with cleaning by ABS were transferred within 5 min after the treatment to prevent surface re-oxidation. An AlN gate insulator of $\simeq$ 19 nm thickness was then deposited on the AlGaN surfaces by RF magnetron sputtering at room temperature with an AlN target in Ar-N_2 ambient. From Hall-effect measurements after the AlN deposition, we obtain electron mobilities $\mu \simeq 900\,cm^2/V\text{-}s$ and $1100\,cm^2/V\text{-}s$ with sheet electron concentrations $n_s \simeq 6.5 \times 10^{12}\,cm^{-2}$ and $7.0 \times 10^{12}\,cm^{-2}$, for the devices with and without cleaning by ABS, respectively, suggesting that the cleaning by ABS leads to further sputtering damage. The formation of Ni/Au gate electrodes completed the device fabrication. As illustrated in Fig. 1, the MIS transistors have the gate length of 250 nm, the source-gate spacing of 2 μm, the gate-drain spacing of 3 μm, and the gate width of 50 μm, while the MIS capacitors have the 100 μm $\times$ 100 μm gate electrode surrounded by the Ohmic electrode.

III. ANALYSIS BY USING CAPACITANCE-FREQUENCY-TEMPERATURE MAPPING

We investigated the AlN/AlGaN/GaN MIS capacitors to analyze the AlN-AlGaN interface states. We measured *C-V-f* characteristics between the gate electrode and the grounded Ohmic electrode surrounding the gate of the MIS capacitors at temperatures from 150 K to 393 K. Figure 2 shows the *C-V-f* characteristics at 150 K, 300 K, and 393 K for the devices with and without cleaning by ABS. At 393 K, for both surface treatments, we observe frequency dispersions at forward gate biases, which are attributed to electron trapping/detrapping at interface states, while the frequency dispersions disappear at 150 K because of long trapping time constants. The device with cleaning by ABS exhibits smaller frequency dispersions at forward biases than the device without the cleaning, suggesting that the cleaning is effective to suppress the frequency dispersions caused by the interface states.

From the temperature-dependent *C-V-f* characteristics, we obtain *C-f-T* mappings with contours for the devices with and without cleaning by ABS as shown in Fig. 3, where the gate voltages V_G are 0 V, 1 V, 2 V, and 3 V. The contours exhibit a straight line behavior, which can be explained by the Lehovec small-signal equivalent circuit of MIS structures. The equivalent circuit is depicted in Fig. 4 (left), which consists of an interface state capacitance C_i, an interface state conductance G_i, and an AlGaN capacitance C_{AlGaN} in parallel, with an AlN capacitance C_{AlN} connected in series. Using the interface state density D_i and the electron trapping time constant τ, we obtain[32]

$$C_i = \frac{q^2 D_i \arctan(\omega\tau)}{\omega\tau} \tag{1}$$

and

$$\frac{G_i}{\omega} = \frac{q^2 D_i \ln(1+\omega^2\tau^2)}{2\omega\tau}, \tag{2}$$

where q is the electron charge and $\omega = 2\pi f$ is the angular frequency, as the basis of the conductance method. Since the total admittance of the equivalent circuit is

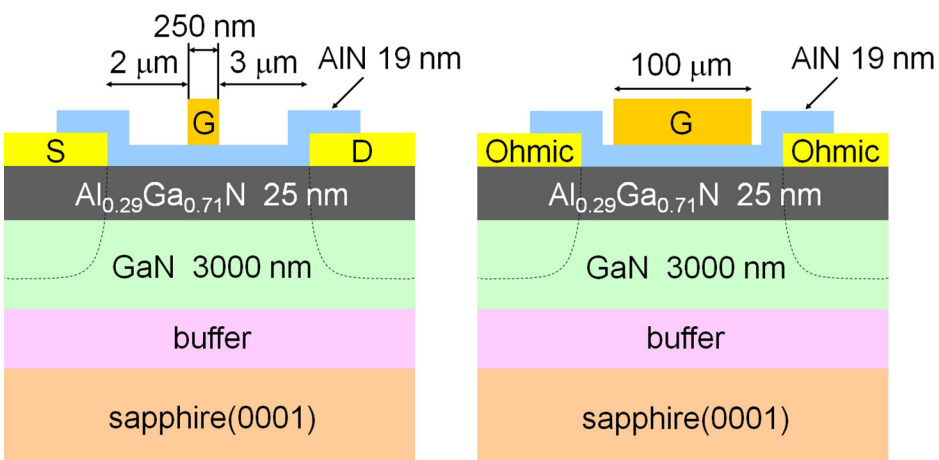

FIG. 1. Schematic cross sections of the fabricated MIS transistors (left) and MIS capacitors (right).

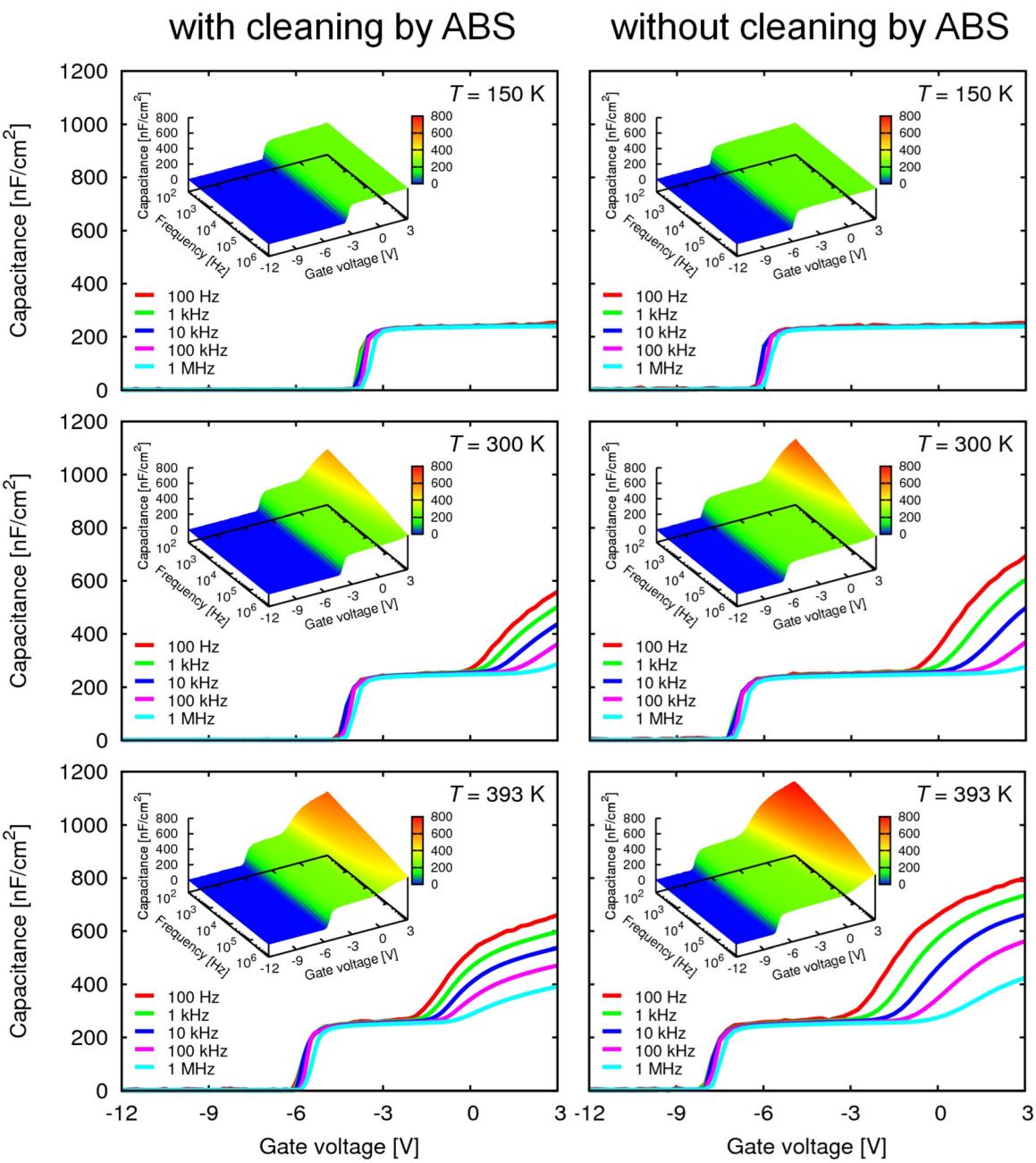

FIG. 2. *C-V-f* characteristics at 150 K, 300 K, and 393 K, of the MIS capacitors with and without cleaning by ABS. Inset: 3-D plots of the *C-V-f* characteristics.

$$Y = \frac{1}{Z} = \left(\frac{1}{jC_{\mathrm{AlN}}\omega} + \frac{1}{G_{\mathrm{i}} + jC_{\mathrm{AlGaN}}\omega + jC_{\mathrm{i}}\omega} \right)^{-1}, \quad (3)$$

with C_{i} given by Eq. (1) and G_{i}/ω by Eq. (2) as functions of only $\omega\tau$, the capacitance given by the imaginary part of the total admittance, $C = \mathrm{Im}Y/\omega$, is a function of only $\omega\tau$. Therefore, a contour in the *C-f-T* mapping, i.e., $C =$ constant leading to $\omega\tau = 2\pi f\tau =$ constant, exhibits a straight line behavior expressed by $f \propto 1/\tau \propto \exp(-\beta E_{\mathrm{a}})$. As a result, we can extract activation energies E_{a} corresponding to interface state energy levels from the mappings.

Figure 5(a) shows the gate voltage dependence of E_{a} extracted from the contours in the *C-f-T* mappings, where E_{a} is illustrated in the band diagram shown in the inset. For both surface treatments, the *C-f-T* mappings give activation energies for a wide range of gate biases, being effective for characterization of deep interface states. It should be noted that, even though peaks of G_{i}/ω as functions of the frequency used in the conductance method are often not detectable because of being located in the very low-frequency region due to long trapping time constants, we can obtain the activation energies from the contours in the *C-f-T* mappings. Since the small gate-voltage change ΔV_{G} is divided into the bandbending change in the gate insulator AlN, ΔV_{AlN}, and that in the semiconductor AlGaN/GaN, $-\Delta E_{\mathrm{a}}/q$, namely $\Delta V_{\mathrm{G}} \simeq \Delta V_{\mathrm{AlN}} - \Delta E_{\mathrm{a}}/q$, we obtain

$$\frac{\Delta V_{\mathrm{AlN}}}{\Delta V_{\mathrm{G}}} - \frac{\Delta E_{\mathrm{a}}}{\Delta(qV_{\mathrm{G}})} \simeq 1. \quad (4)$$

From the activation energies E_{a} depending on the gate voltage V_{G} given in Fig. 5(a), we obtain the gate-control

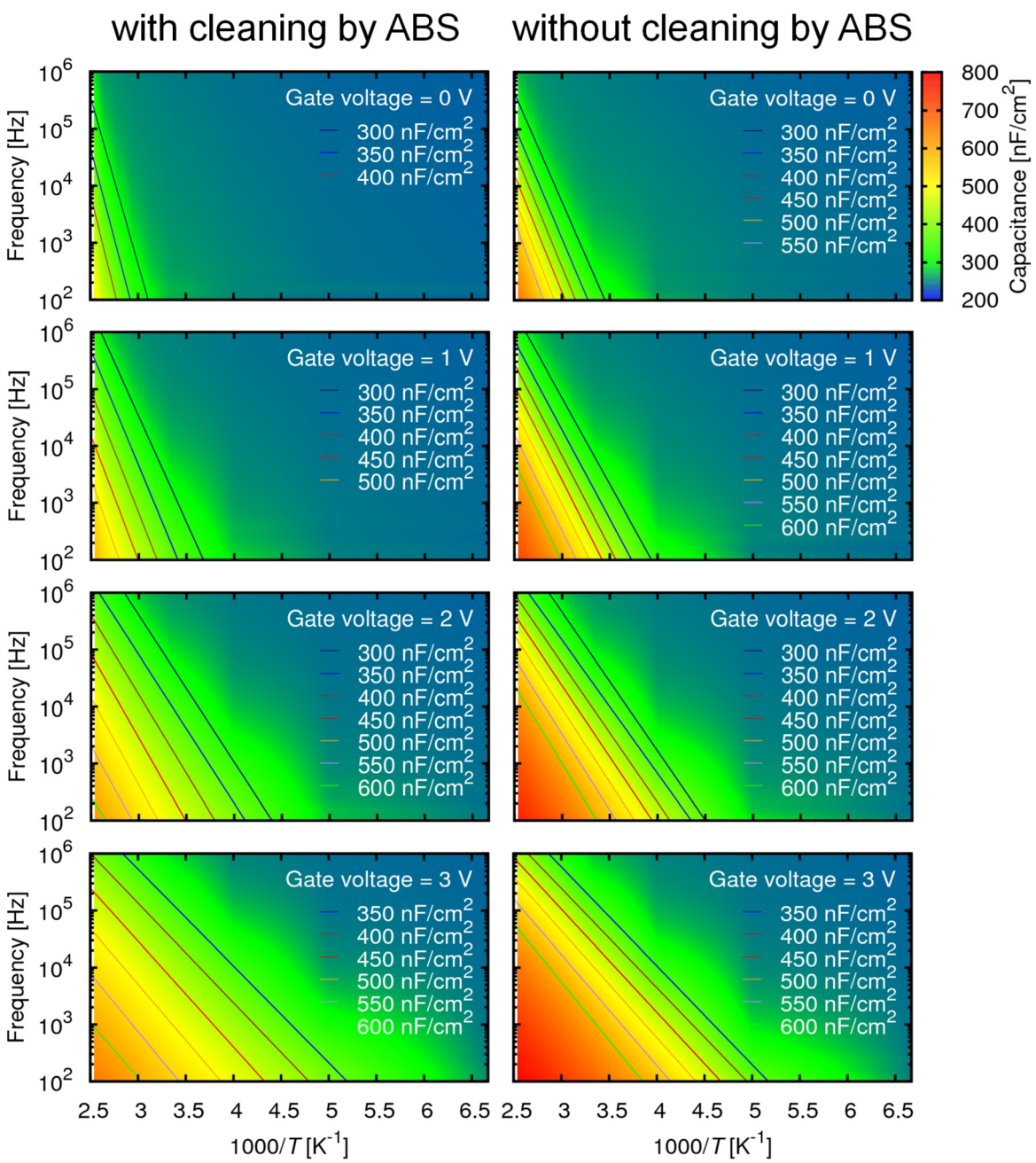

FIG. 3. *C-f-T* mappings with contours at gate voltages V_G of 0 V, 1 V, 2 V, and 3 V, of the MIS capacitors with and without cleaning by ABS.

efficiencies $\xi = -\Delta E_a / \Delta(qV_G)$ as shown in Fig. 5(b), i.e., the ratio of the bandbending change in the semiconductor to the total gate voltage change. In the AC case, a small-signal gate voltage Δv_G is divided into the bandbending in the gate insulator AlN, Δv_{AlN}, and that in the semiconductor AlGaN/GaN according to the equivalent circuit shown in Fig. 4 (left). The ratio $\Delta v_{AlN}/\Delta v_G$ is given by the ratio between the impedance $Z_{AlN} = (jC_{AlN}\omega)^{-1}$ and the total impedance $Z_{total} = Z_{AlN} + [G_i + j(C_{AlGaN} + C_i)\omega]^{-1}$, expressed as

$$\frac{\Delta v_{AlN}}{\Delta v_G} = \frac{Z_{AlN}}{Z_{total}} = \frac{G_i/\omega + j(C_{AlGaN} + C_i)}{G_i/\omega + j(C_{AlN} + C_{AlGaN} + C_i)}. \quad (5)$$

In the DC limit $\omega \to 0$, we obtain $C_i \to q^2 D_i$ and $G_i/\omega \to 0$, leading to the equivalent circuit shown in Fig. 4 (right), and

$$\frac{\Delta v_{AlN}}{\Delta v_G} \to \frac{\Delta V_{AlN}}{\Delta V_G} = \frac{C_{AlGaN} + q^2 D_i}{C_{AlN} + C_{AlGaN} + q^2 D_i} = 1 - \xi \quad (6)$$

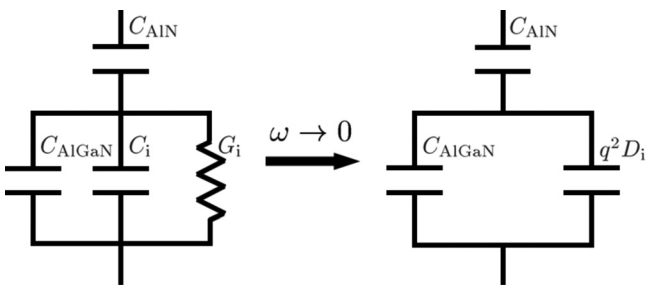

FIG. 4. The Lehovec small-signal equivalent circuit of the MIS capacitors and its DC limit.

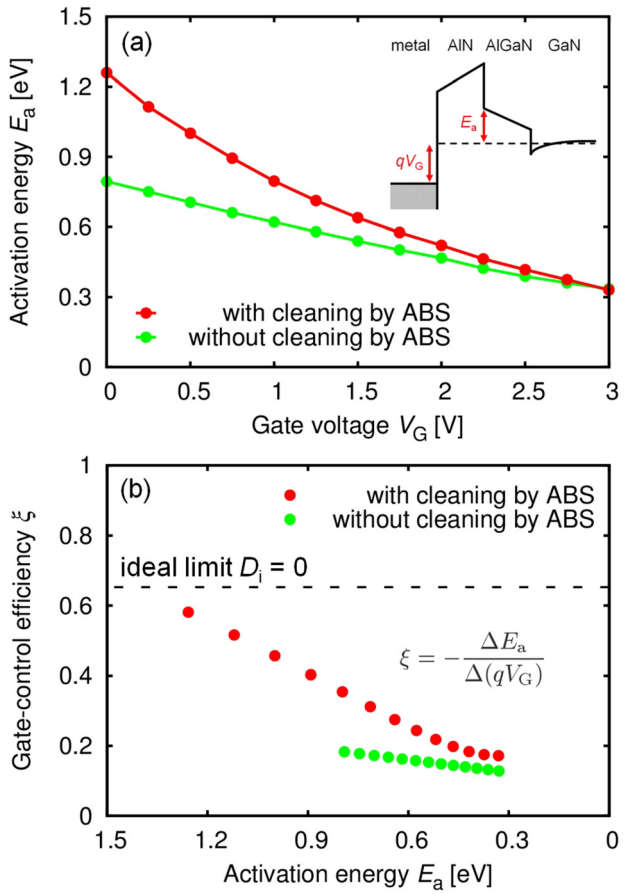

FIG. 5. (a) Gate voltage V_G dependence of activation energies E_a extracted from the contours in the *C-f-T* mappings for the MIS capacitors with and without cleaning by ABS. Inset: illustration of E_a in the band diagram. (b) Gate-control efficiencies $\xi = -\Delta E_a/\Delta(qV_G)$ as functions of E_a.

or

$$\xi = \frac{C_{AlN}}{C_{AlN} + C_{AlGaN} + q^2 D_i}. \quad (7)$$

Using the designed values of $C_{AlN} \simeq 610\,\mathrm{nF/cm^2}$ and $C_{AlGaN} \simeq 325\,\mathrm{nF/cm^2}$ (by separate experiments, it is confirmed that frequency dependence of them is insignificant), gate-control efficiency $\xi \simeq 0.65$ is obtained in the ideal limit

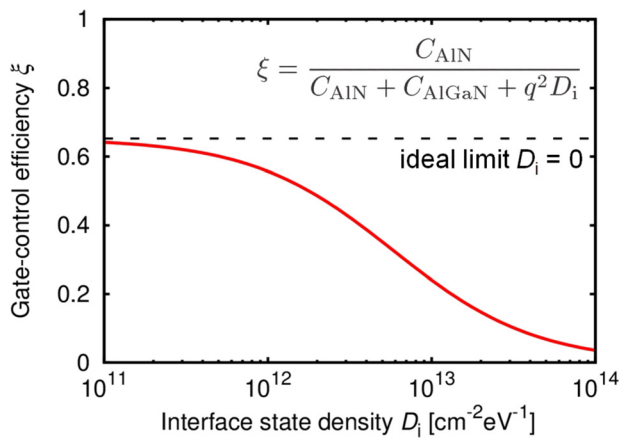

FIG. 6. Calculated results of the gate-control efficiency ξ as a function of the interface state density D_i.

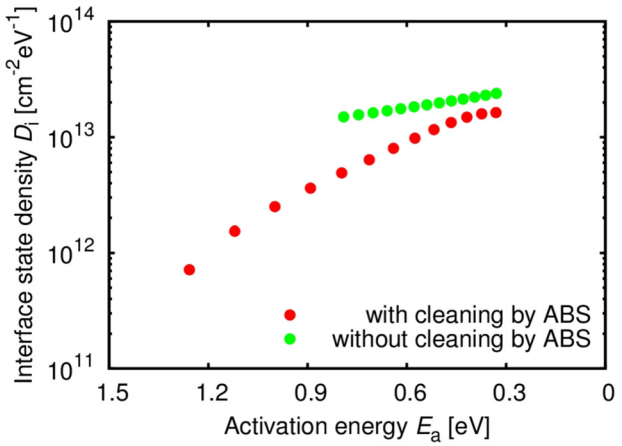

FIG. 7. Interface state densities D_i as functions of E_a for the MIS capacitors with and without cleaning by ABS.

of $D_i = 0$, as indicated by the broken line in Fig. 5(b). However, in reality, ξ is smaller than the ideal value $\simeq 0.65$ as shown in Fig. 5(b) owing to the non-zero D_i. Figure 6 shows the calculated ξ as a function of D_i using Eq. (7). Therefore, from the experimentally obtained gate-control efficiencies ξ in Fig. 5(b), we can evaluate the interface state densities D_i as shown in Fig. 7. We obtain $D_i \sim 10^{12}$-$10^{13}\,\mathrm{cm^{-2}\,eV^{-1}}$ and $\gtrsim 10^{13}\,\mathrm{cm^{-2}eV^{-1}}$ for the devices with and without cleaning by ABS, respectively, for interface

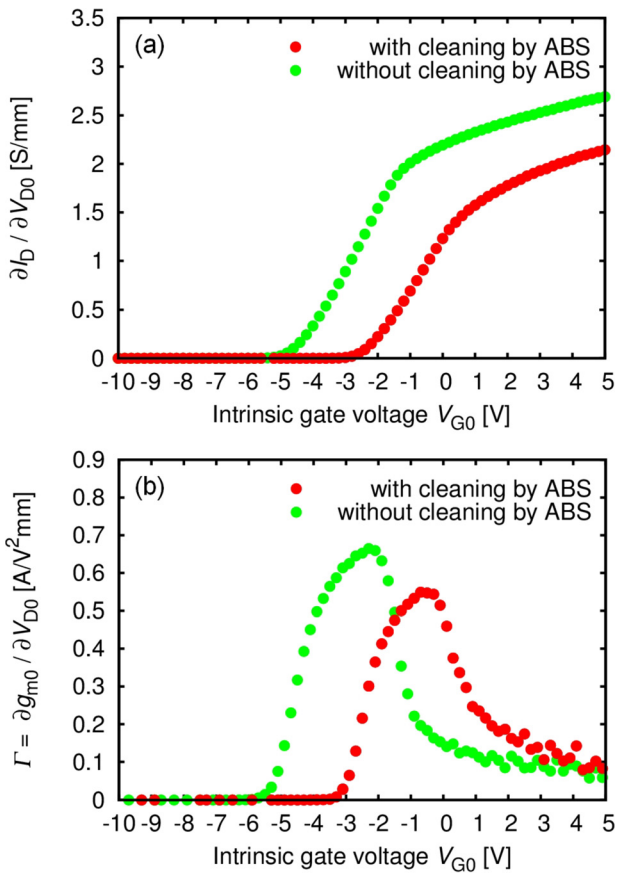

FIG. 8. Linear-region characteristics of the MIS transistors with and without cleaning by ABS. (a) $\partial I_D/\partial V_{D0}$ and (b) $\Gamma = \partial g_{m0}/\partial V_{D0}$ as an indicator of the linear-region intrinsic transconductance g_{m0}, as functions of intrinsic gate voltage V_{G0}.

state energy levels $\lesssim 1$ eV below the AlGaN conduction band edge. While the conductance method was available only for interface state energy levels $\lesssim 0.4$ eV below the AlGaN conduction band edge,[7] the *C-f-T* mapping method enables us to analyze deeper interface states in wide-bandgap MIS devices. Although the obtained D_i for $\lesssim 0.4$ eV below the AlGaN conduction band edge is smaller than that by the conductance method, we suppose an overestimation by the conductance method with a leakage conductance. Since the real part of the admittance of the equivalent circuit is modified by the leakage conductance,[33] the result of the conductance method, which mainly utilizes the real part, is significantly influenced, whereas the present method based on the imaginary part has immunity to the influence. As shown in Fig. 7, the interface state densities increase with the decrease in E_a, corresponding to the shallower interface state energy levels near the AlGaN conduction band edge. According to this, the gate-control efficiencies in Fig. 5(b) decrease with decrease in E_a, owing to the high-density interface states. The device with cleaning by ABS exhibits a better gate-control efficiency and a lower interface state density than the device without the cleaning; the cleaning is effective for reduction of the interface state density and improvement of the gate-control efficiency.

In the following, we consider transconductances of the AlN/AlGaN/GaN MIS transistors in relation with the gate-control efficiencies and the interface state densities. We focus on the linear-region transconductances of the MIS transistors because the gate-control efficiencies and the interface state densities are obtained from the MIS capacitors, whose electric potential conditions are close to those in the linear region of the MIS transistors. Moreover, it is necessary to investigate the intrinsic transconductances of the MIS transistors excluding the effects of source resistance R_S and drain resistance R_D. With the source grounded, we define the intrinsic gate voltage $V_{G0} = V_G - R_S I_D$ and the intrinsic drain voltage $V_{D0} = V_D - (R_S + R_D) I_D$, where I_D is the drain current and V_D is the drain voltage. Figure 8(a) shows $\partial I_D / \partial V_{D0}$ as functions of V_{G0} in the linear region of the MIS transistors. In Fig. 8(b), we plot

$$\Gamma = \frac{\partial^2 I_D}{\partial V_{D0} \partial V_{G0}} = \frac{\partial g_{m0}}{\partial V_{D0}} \tag{8}$$

depending on V_{G0}, as an indicator of the linear-region intrinsic transconductance g_{m0}. The device with cleaning by ABS exhibits a lower peak Γ than the device without the cleaning, owing to the larger sputtering damage, which reduces the electron mobility and sheet electron concentration, leading to the large sheet resistance. The shallower threshold voltage for the device with cleaning by ABS is also attributed to the larger damage. However, for the forward biases, the device with cleaning by ABS exhibits higher Γ, owing to the better gate-control efficiency and the lower interface state density.

Regarding V_{G0} as the gate voltage in Fig. 5(a), we obtain Γ as functions of E_a for the MIS transistors with and without cleaning by ABS, as shown in Fig. 9(a). We find that the intrinsic transconductances decrease with the decrease in E_a,

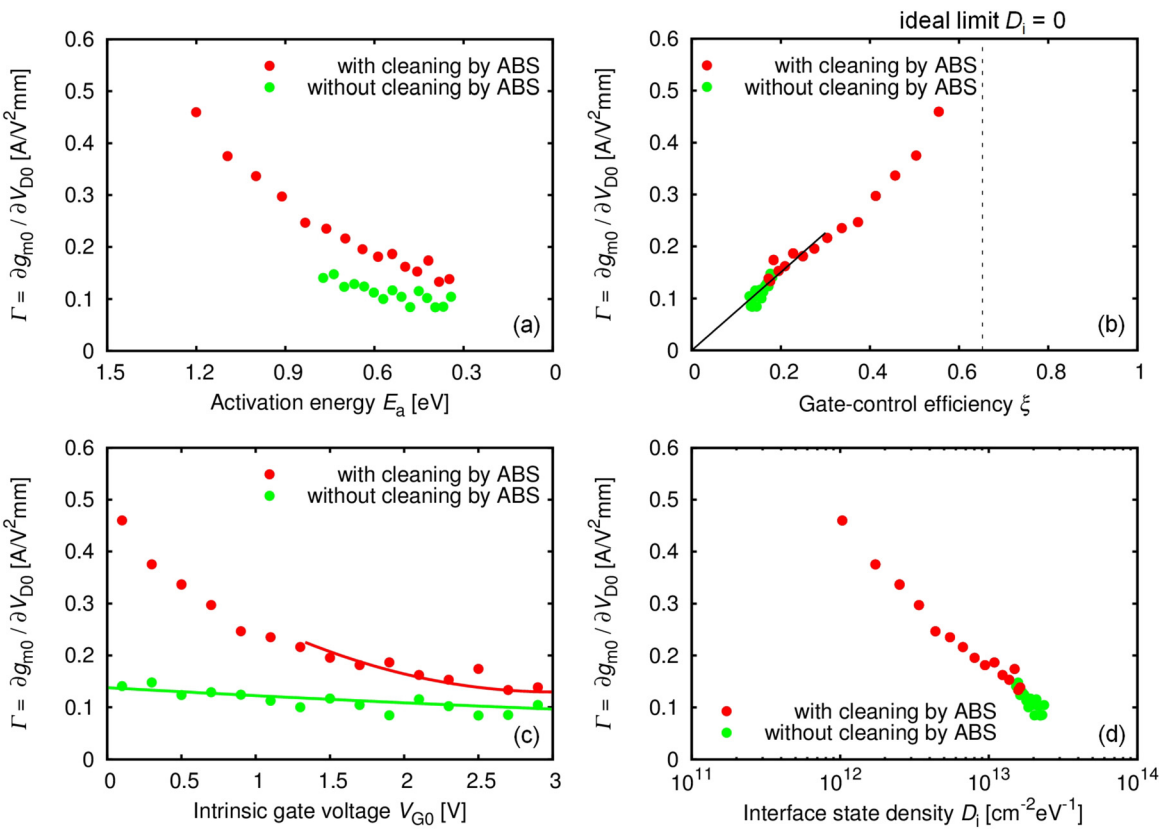

FIG. 9. Relations between Γ and (a) the activation energy E_a, (b) the gate-control efficiencies ξ, (c) the intrinsic gate voltage V_{G0}, and (d) the interface state densities D_i, for the MIS devices with and without cleaning by ABS.

owing to the high-density interface states near the AlGaN conduction band edge. The device with cleaning by ABS exhibits a larger Γ than the device without the cleaning; the cleaning is effective for improvement of the intrinsic transconductance. The behaviors of the intrinsic transconductances in Fig. 9(a) have a close resemblance to those of the gate-control efficiencies ξ in Fig. 5(b). From the E_a-dependence of ξ and Γ, we obtain the correlation shown in Fig. 9(b); the intrinsic transconductances increase as the gate-control efficiencies increase. For the low-Γ (low-ξ) regime, a linear relation between Γ and ξ is obtained by fitting, as shown by the solid line in Fig. 9(b). Assuming a constant mobility μ, from its definition of Eq. (8), Γ is given by

$$\Gamma = \frac{\mu}{L_G}\frac{\partial(qn_s)}{\partial V_{G0}} = \frac{\mu}{L_G}\frac{\dfrac{C_{AlGaN}}{C_{AlGaN}+q^2D_i}}{\dfrac{1}{C_{AlN}}+\dfrac{1}{C_{AlGaN}+q^2D_i}} = \frac{\mu}{L_G}\frac{C_{AlGaN}C_{AlN}}{C_{AlN}+C_{AlGaN}+q^2D_i} = \frac{\mu}{L_G}C_{AlGaN}\xi, \quad (9)$$

where L_G is the gate length. From this and the linear relation between Γ and ξ obtained by the fitting, we extract the mobility $\mu \sim 580\,cm^2/V\text{-}s$ using the values of C_{AlGaN} and L_G. Applying this mobility, we can reproduce the relation between Γ and ξ for low-Γ regime as shown in Fig. 9(c). This mobility is lower than those obtained by the Hall-effect measurements after the AlN deposition, owing to significant AlGaN-GaN interface roughness scattering[34] at high sheet electron concentrations corresponding to forward gate biases. Moreover, the intrinsic transconductances are correlated with the interface state densities D_i in Fig. 7; from the E_a-dependence of Γ and D_i, we obtain the correlation shown in Fig. 9(d), where the intrinsic transconductances decrease with increase in the interface state densities.

IV. XPS CHARACTERIZATION OF AlN-AlGaN INTERFACES

To investigate the origin of the properties depending on the AlN-AlGaN interface formation processes, revealed by the above analysis, we employed four samples illustrated in the insets of Fig. 10, for XPS characterization of the AlGaN surfaces and the AlN-AlGaN interfaces. The four samples were prepared according to the device fabrication processes. Samples (a) (AlGaN with ABS) and (b) (AlGaN without ABS) are the

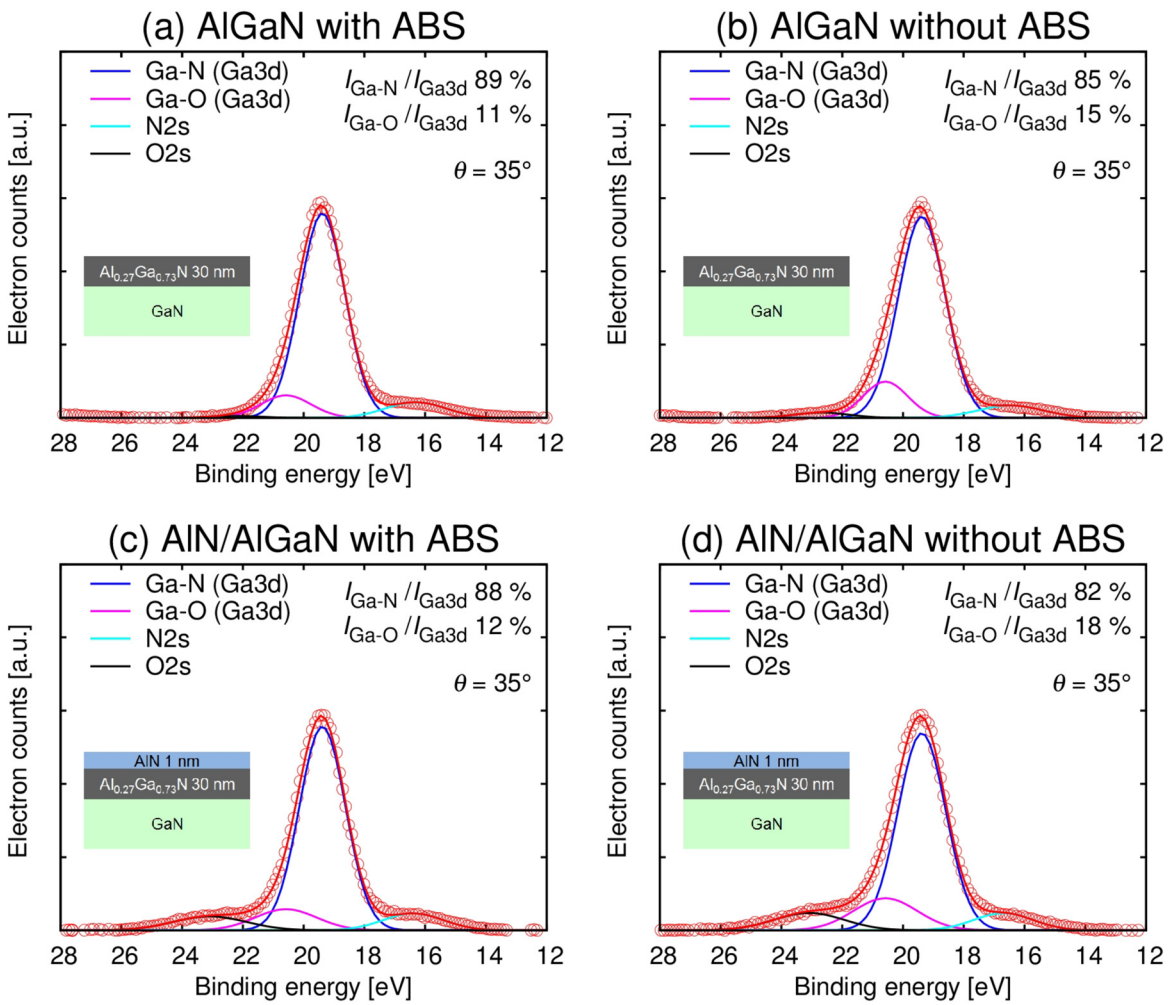

FIG. 10. Ga3d, N2s, and O2s peaks measured at a take-off angle $\theta = 35°$ for the samples (a) AlGaN with ABS, (b) AlGaN without ABS, (c) AlN/AlGaN with ABS, and (d) AlN/AlGaN without ABS, where $I_{Ga\text{-}O}/I_{Ga3d}$ ($I_{Ga\text{-}N}/I_{Ga3d}$) is the ratio of the integrated peak intensity of Ga-O (Ga-N) bonding component to that of the total Ga3d peak. Insets: illustration of the samples for XPS characterization.

AlGaN/GaN heterostructures treated by organic cleaning with and without the additional cleaning by ABS for the AlGaN surfaces, respectively. Samples (c) (AlN/AlGaN with ABS) and (d) (AlN/AlGaN without ABS) are obtained by AlN ~1 nm deposition on the AlGaN surfaces treated by the processes of samples (a) and (b), respectively. The samples (a) and (b) are for investigation of the AlGaN surfaces with different treatments. On the other hand, the samples (c) and (d) are for investigation of the AlN-AlGaN interfaces formed by the AlN deposition on the AlGaN surfaces with different treatments, their XPS spectra including information of not only the AlN surfaces but also the AlN-AlGaN interfaces owing to the thin AlN. All samples were introduced to the XPS chamber within 20 min after they were prepared, followed by XPS measurements using take-off angles $\theta = 25°$-$75°$. Figure 10 shows Ga3d, N2s, and O2s peaks measured at $\theta = 35°$. The O2s peak intensities increase for the samples (c) and (d) compared to those for the samples (a) and (b), respectively, owing to natural oxidation of the AlN. The Ga3d peaks are decomposed into the Ga-O and Ga-N bondings. We obtain the ratio of the integrated peak intensity of the Ga-O (Ga-N) bonding component to that of the total Ga3d peak, $I_{\text{Ga-O}}/I_{\text{Ga3d}}$ ($I_{\text{Ga-N}}/I_{\text{Ga3d}}$). Although the Ga-N bonding components dominate the Ga3d peaks, we can observe differences in $I_{\text{Ga-O}}/I_{\text{Ga3d}}$ depending on the treatments; the samples (a) and (c) exhibit smaller $I_{\text{Ga-O}}/I_{\text{Ga3d}} \simeq 11$-$12\,\%$, than $I_{\text{Ga-O}}/I_{\text{Ga3d}} \simeq 15$-$18\,\%$ of the samples (b) and (d). In Fig. 11, we show $I_{\text{Ga-O}}/I_{\text{Ga3d}}$ for other take-off angles also exhibiting smaller values for the samples (a) and (c) than for the samples (b) and (d), respectively. The AlGaN surface cleaning by ABS before the AlN deposition removes the initial oxide layer, leading to less Ga-O bonding and the lower interface state density, giving the better gate-control efficiency and the higher intrinsic transconductance of the MIS devices. These results indicate that, Ga-O bonding plays an important role in the AlN-AlGaN interfaces, similarly to the importance of Ga-O bonding in Al_2O_3-AlGaN interfaces.[35]

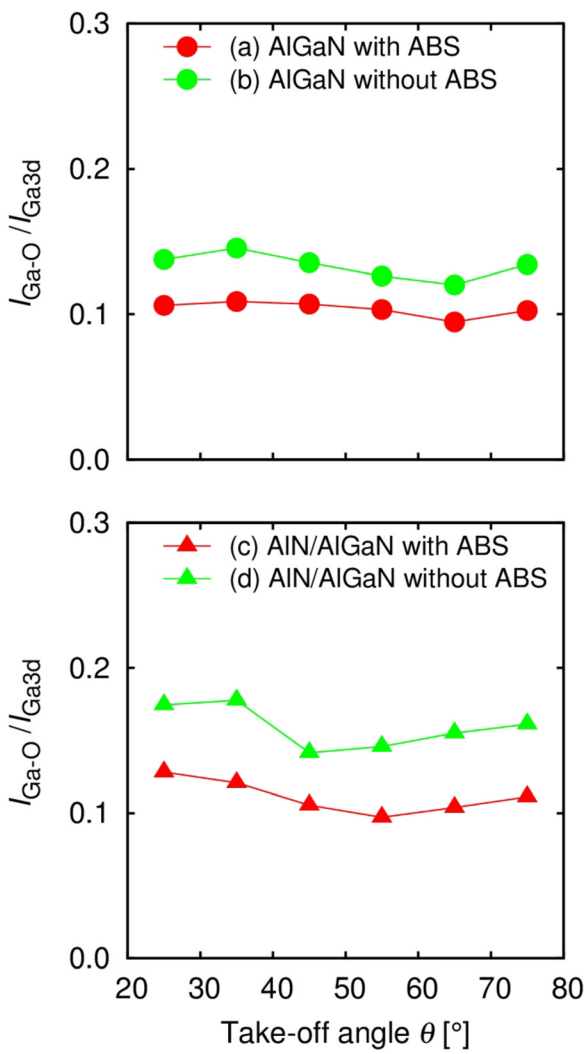

FIG. 11. $I_{\text{Ga-O}}/I_{\text{Ga3d}}$ and $I_{\text{Ga-N}}/I_{\text{Ga3d}}$ at $\theta = 25°$-$75°$ for the samples (a) AlGaN with ABS, (b) AlGaN without ABS, (c) AlN/AlGaN with ABS, and (d) AlN/AlGaN without ABS.

V. CONCLUSION

We presented the analysis method by using the *C-f-T* mappings to evaluate the gate-control efficiencies and the interface state densities for AlN/AlGaN/GaN MIS devices with different formation processes of the AlN-AlGaN interfaces. From the constant-capacitance contours in the mappings, we extracted the gate-bias-dependent activation energies, whose derivative gives the gate-control efficiencies. Considering the DC limit of the Lehovec small-signal equivalent circuit and using the experimentally obtained gate-control efficiencies, we evaluated the interface state densities depending on the interface formation processes for energy levels $\lesssim 1$ eV below the AlGaN conduction band edge. The analysis method by using *C-f-T* mapping enables us to analyze deep interface states in wide-bandgap MIS devices, in comparison with the conductance method. Moreover, it was shown that the gate-control efficiencies and the interface state densities have correlations with the linear-region intrinsic transconductances, all depending on the interface formation processes. In addition, we characterized the AlN-AlGaN interfaces by using XPS, in relation with the results of the analysis. It is indicated that Ga-O bonding plays an important role in the AlN-AlGaN interfaces; removal of the initial oxide layer leads to less Ga-O bonding, the lower interface state density, the better gate-control efficiency, and the higher intrinsic transconductance of the MIS devices.

[1]T. Hashizume, S. Ootomo, and H. Hasegawa, Appl. Phys. Lett. **83**, 2952 (2003).
[2]C. Liu, E. F. Chor, and L. S. Tan, Appl. Phys. Lett. **88**, 173504 (2006).
[3]A. Kawano, S. Kishimoto, Y. Ohno, K. Maezawa, T. Mizutani, H. Ueno, T. Ueda, and T. Tanaka, Phys. Status Solidi C **4**, 2700 (2007).
[4]Y. Liu, J. A. Bardwell, S. P. McAlister, S. Rolfe, H. Tang, and J. B. Webb, Phys. Status Solidi C **0**, 69 (2002).
[5]R. Stoklas, D. Gregušová, Š. Gaži, J. Novák, and P. Kordoš, J. Vac. Sci. Technol. B **29**, 01A809 (2011).
[6]H.-A. Shih, M. Kudo, M. Akabori, and T. Suzuki, Jpn. J. Appl. Phys. **51**, 02BF01 (2012).
[7]H.-A. Shih, M. Kudo, and T. Suzuki, Appl. Phys. Lett. **101**, 043501 (2012).
[8]S. P. Le, T. Q. Nguyen, H.-A. Shih, M. Kudo, and T. Suzuki, J. Appl. Phys. **116**, 054510 (2014).
[9]J.-C. Gerbedoen, A. Soltani, M. Mattalah, M. Moreau, P. Thevenin, and J.-C. D. Jaeger, Diamond Relat. Mater. **18**, 1039 (2009).
[10]T. Q. Nguyen, H.-A. Shih, M. Kudo, and T. Suzuki, Phys. Status Solidi C **10**, 1401 (2013).

[11]J. Hwang, W. Schaff, B. Green, H. Cha, and L. Eastman, Solid-State Electron. **48**, 363 (2004).
[12]N. Tanaka, H. Takita, Y. Sumida, and T. Suzuki, Phys. Status Solidi C **5**, 2972 (2008).
[13]N. Tanaka, Y. Sumida, H. Kawai, and T. Suzuki, Jpn. J. Appl. Phys. **48**, 04C099 (2009).
[14]N. Tsurumi, H. Ueno, T. Murata, H. Ishida, Y. Uemoto, T. Ueda, K. Inoue, and T. Tanaka, IEEE Trans. Electron Devices **57**, 980 (2010).
[15]S. Huang, Q. Jiang, S. Yang, C. Zhou, and K. Chen, IEEE Electron Device Lett. **33**, 516 (2012).
[16]E. J. Miller, X. Z. Dang, H. H. Wieder, P. M. Asbeck, E. T. Yu, G. J. Sullivan, and J. M. Redwing, J. Appl. Phys. **87**, 8070 (2000).
[17]R. M. Chu, Y. G. Zhou, K. J. Chen, and K. M. Lau, Phys. Status Solidi C **0**, 2400 (2003).
[18]L. Semra, A. Telia, and A. Soltani, Surf. Interface Anal. **42**, 799 (2010).
[19]B. Gaffey, L. Guido, X. Wang, and T. Ma, IEEE Trans. Electron Devices **48**, 458 (2001).
[20]R. Stoklas, D. Gregušová, J. Novák, A. Vescan, and P. Kordoš, Appl. Phys. Lett. **93**, 124103 (2008).
[21]J. J. Freedsman, T. Kubo, and T. Egawa, Appl. Phys. Lett. **99**, 033504 (2011).
[22]Y. Chiou, S. Chang, Y. Su, C. Wang, T. Lin, and B.-R. Huang, IEEE Trans. Electron Devices **50**, 1748 (2003).
[23]M. Miczek, C. Mizue, T. Hashizume, and B. Adamowicz, J. Appl. Phys. **103**, 104510 (2008).
[24]Y. Q. Wu, T. Shen, P. Ye, and G. Wilk, Appl. Phys. Lett. **90**, 143504 (2007).
[25]C. Mizue, Y. Hori, M. Miczek, and T. Hashizume, Jpn. J. Appl. Phys. **50**, 021001 (2011).
[26]T. Mizutani, H. Makihara, M. Akita, Y. Ohno, S. Kishimoto, and K. Maezawa, Jpn. J. Appl. Phys. **42**, 424 (2003).
[27]M. Faqir, G. Verzellesi, F. Fantini, F. Danesin, F. Rampazzo, G. Meneghesso, E. Zanoni, A. Cavallini, A. Castaldini, N. Labat, A. Touboul, and C. Dua, Microelectron. Reliab. **47**, 1639 (2007).
[28]Y. Nakano and T. Jimbo, Appl. Phys. Lett. **80**, 4756 (2002).
[29]T. Okino, M. Ochiai, Y. Ohno, S. Kishimoto, K. Maezawa, and T. Mizutani, IEEE Electron Device Lett. **25**, 523 (2004).
[30]G. Brammertz, K. Martens, S. Sioncke, A. Delabie, M. Caymax, M. Meuris, and M. Heyns, Appl. Phys. Lett. **91**, 133510 (2007).
[31]P. Kordoš, R. Stoklas, D. Gregušová, Š. Gaži, and J. Novák, Appl. Phys. Lett. **96**, 013505 (2010).
[32]K. Lehovec, Appl. Phys. Lett. **8**, 48 (1966).
[33]T. Ma and R. Barker, Solid-State Electron. **17**, 913 (1974).
[34]J. Antoszewski, M. Gracey, J. Dell, L. Faraone, T. A. Fisher, G. Parish, Y. Wu, and U. Mishra, J. Appl. Phys. **87**, 3900 (2000).
[35]X. Qin, A. Lucero, A. Azcatl, J. Kim, and R. M. Wallace, Appl. Phys. Lett. **105**, 011602 (2014).